Journal of Alloys and Compounds 509 (2011) 7253–7258

Contents lists available at ScienceDirect

Journal of Alloys and Compounds

journal homepage: www.elsevier.com/locate/jallcom

Thermal treatment effect on structure, electrical conductivity and transient photoconductivity behavior of thiourea modified TiO_2 sol–gel thin films

K. Pomoni [a,*], A. Vomvas [a], N. Todorova [b], T. Giannakopoulou [b], K. Mergia [c], C. Trapalis [b]

[a] Department of Physics, University of Patras, 26504 Patras, Greece
[b] Institute of Materials Science, National Centre for Scientific Research "Demokritos" 15310, Ag. Paraskevi, Attikis, Greece
[c] Institute of Nuclear Technology and Radiation Protection, National Centre for Scientific Research "Demokritos" 15310, Ag. Paraskevi, Attikis, Greece

ARTICLE INFO

Article history:
Received 30 November 2010
Received in revised form 23 March 2011
Accepted 28 March 2011
Available online 5 April 2011

Keywords:
N and S co-doped TiO_2
Dark conductivity
Transient photoconductivity
Sol–gel
Nanocrystalline
UV–vis

ABSTRACT

Thiourea modified nanocrystalline titanium dioxide (TiO_2) thin films were prepared by sol–gel route and were thermally treated at five different temperatures (400, 500, 600, 800 and 1000 °C). The films were studied using GIXRD, PIGE and UV–vis spectroscopy. It was observed that the anatase to rutile phase transformation of TiO_2 was inhibited by the thiourea modification. The transmittance of the modified films appeared reduced which was attributed both to the modification of TiO_2 with thiourea and the light scattering in the films. The dark conductivity and the transient photoconductivity of the modified TiO_2 sol–gel thin films were studied in vacuum and in air. The environment does not influence significantly the dark conductivity, because of the almost equivalent competition between oxygen and water adsorption. The photoconductivity reaches high values for all samples in both environments, with the sample treated at 500 °C to present the highest value. The larger values in vacuum can be attributed to the reduced amount of adsorbed oxygen at the surface, which acts as electron scavenger.

1. Introduction

Titanium dioxide (TiO_2) has been the focus of extensive studies in recent years in view of its various applications in electrochromics, photocatalysis as well as gas in sensing and photovoltaic devices [1]. Several of the technological applications depend on the remarkable electrical properties and photocatalytic activity of TiO_2. The temperature dependence of the conductivity can provide fundamental information on charge transport mechanisms and activation energy, useful for optimizing the properties of various devices [2]. The electrical properties of TiO_2 can be controlled either by oxygen vacancies or by doping. It is well known that incorporation of Niobium into TiO_2 results in the enhancement of the electrical conductivity of TiO_2 [3–6]. Dopants like Fe [7,8], Ni [9], Cr [10] have been used to control the electrical properties of TiO_2. However, the effect of doping with anionic species like N, S, F and B to the conductivity behavior has not sufficiently studied [11–13].

In photocatalytic applications, doping of pure TiO_2 with foreign atoms has been widely investigated. TiO_2 photocatalyst is activated only by UV light irradiation, because of its large band gap, which is around 3.0 eV for rutile and 3.2 eV for anatase phase. Doping is one of the typical approaches adopted to extend the absorption edge of TiO_2 to the visible region, in order to take advantage of the main part of the solar spectrum. It has been shown that modification of TiO_2 using transition metals can shift the optical absorption edge of TiO_2 from the ultraviolet to the visible range [14–18]. However, metal-doping into TiO_2 causes thermal instability and low quantum efficiency of the photoinduced charge carriers [19–21].

Over the last several years, the doping of TiO_2 with non-metal elements has received much attention [22–37]. The substitution of oxygen in TiO_2 with anionic species like N, C, S or F leads to a band gap narrowing and a higher photocatalytic activity under visible light. Namely, N- and S-doped TiO_2 are considered excellent candidates, since they exhibit enhanced photoactivity under visible light irradiation due to the shift of the absorption edge to a lower energy [22,24,25,29,31–33,35–37]. Some research groups report that the observed band-gap narrowing can be attributed to the mixing of N 2p states with TiO_2 valence band (VB) or S 3p states with TiO_2 VB [22,24]. Alternatively, it is considered that the dopants introduce additional isolated states above the VB [38–41] or on both the above mentioned mixing and the induced states above VB [42]. The co-doping of non-metal elements within the oxide lattice has attracted considerable interest. A remarkable improvement in activity, mainly arisen from a red shift in the absorption edge, as well as a great enhancement of photocatalytic behavior have been reported for N and S co-doped TiO_2 and are both attributed to the cooperative action of the dopants. The use of thiourea as a precursor for the simultaneous N and S doping of TiO_2 catalyst has also been studied [21,43,44].

* Corresponding author. Tel.: +30 2610 997482; fax: +30 2610 997451.
E-mail address: pomoni@physics.upatras.gr (K. Pomoni).

0925-8388/$ – see front matter © 2011 Elsevier B.V. All rights reserved.
doi:10.1016/j.jallcom.2011.03.152

The sol–gel technique has been adopted as one of the best methods for the preparation of metal and non-metal doped nanocrystalline TiO_2 because of its advantages, such as purity, homogeneity and flexibility in introducing dopants in large concentrations [45]. In recent reports, non-metal doped TiO_2 materials synthesized by the sol–gel method have been investigated towards their photocatalytic activity under UV and visible light illumination, as well as their structural, optical, and other properties [35,46,47].

Although widespread applications of TiO_2 are credited to its high level of photoconductivity [36], up to now, the conductivity and the photoconductivity of non-metal doped TiO_2 materials in different environments have been poorly studied. Based on the literature review, no research effort has been devoted to the conductivity and transient photoconductivity study of sol–gel nanostructured N and S co-doped TiO_2 films using modification with thiourea.

In this work, we present our results on processing and on structural, electrical and photoconductive properties of thiourea modified sol–gel TiO_2 thin films. Furthermore, the influence of the thermal treatment of the films and of the environment on the conductivity and photoconductivity is discussed.

2. Experimental details

2.1. Preparation of thiourea modified sol–gel TiO_2 thin films

Modified TiO_2 thin films on Quartz substrate were prepared by sol–gel route. Tetrabutylorthotitanate (TBOTi), Fluca, and thiourea, Acros Organics, were used as Ti precursor and modification agent respectively. Ethanol absolute (Eth), Panreac, was used as solvent in molar ratio Eth/TBOTi = 40. The quantity of thiourea was calculated towards Ti in S/Ti = 1/1 atomic ratio. The thiourea was dissolved in the alcohol and the solution was stirred in a closed round bottom flask for 40 min at room temperature. Then, the TBOTi was added and the stirring was continued for 16 h under the same conditions. The resultant transparent, stable, light-yellow solution was used for dip-coating deposition on Quartz Plates 50 mm × 10 mm × 1 mm. The dipping process was performed at constant speed of 3.33×10^{-3} m/s. The obtained gel films were thermally treated in air for 1 h at different temperatures, namely 400, 500, 600, 800 and 1000 °C. A "Carbolite" muffle furnace was used with a heating rate of 5 °C/min. All films appeared semitransparent and white in color. The thickness of the films was determined by talystep profilometer and found to be 100, 92, 89, 86 and 80 nm for the samples treated at 400, 500, 600, 800 and 1000 °C, respectively.

2.2. Grazing incidence X-ray diffraction (GIXRD) and UV–vis spectroscopy

The GIXRD measurements were performed on a D8 Advance Bruker diffractometer using CuKα radiation and a parallel beam stemming from a Göbel mirror. The average size of the crystallites was determined using the Scherrer's semi-empirical equation for the stronger Bragg peak

$$d = \frac{K\lambda}{\beta \cos\theta} \quad (1)$$

where λ is the wavelength of X-rays (0.154 nm), β is the full width at half maximum of the peak in radian, θ is the Bragg angle, and $K = 0.9$. In Eq. (1), the instrumental line broadening was subtracted in order to take into account only the peak broadening due to the sample.

The phase content (%) of the samples was calculated from the integrated intensities of anatase (1 0 1) and rutile (1 1 0) peaks using the Spurr equation [48]

$$W_R = \frac{I_R(1\ 1\ 0)}{0.8I_A(1\ 0\ 1) + I_R(1\ 1\ 0)} \quad (2)$$

where I_A (1 0 1) and I_R (1 1 0) are the stronger peak intensities of anatase and rutile respectively, and W_R is the rutile mass fraction.

UV–visible transmittance spectra of the samples were recorded using UV-2100 Shimadzu spectrophotometer in the wavelength range of 200–900 nm.

2.3. Electrical conductivity and photoconductivity measurements

For the electrical conductivity and photoconductivity measurements, coplanar silver electrodes with a distance of 0.8 mm were vacuum deposited on the samples. A vacuum cryostat was used, while the temperature was adjusted by an Oxford ITC502S temperature controller. A constant bias voltage of 5 V was applied to the samples, since no deviation from linearity in current–voltage curves was observed in the voltage range 1–10 V. A 100 W (white light) Xenon lamp was used as light source for the transient photoconductivity measurements. The white light was heat filtered and the full light intensity at the samples' surface was set to 500 W/m^2 by means of a calibrated Si-photodiode of known quantum efficiency. The light was switched on and off in 20 min intervals. The photocurrent response was measured by a Keithley 617 electrometer and recorded every 10 s by means of a computer via IEEE-488 bus. Before measurement, the samples were annealed at 440 K for 90 min and left to cool down, for the elimination of persisting effects of previous light exposure. Consequently, the samples remained in the dark for 24 h at room temperature before performing the photoconductivity measurements.

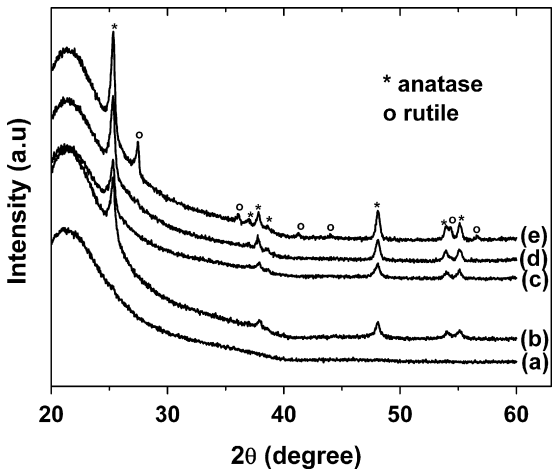

Fig. 1. GIXRD patterns of the thiourea modified TiO_2 samples, treated at: (a) 400 °C, (b) 500 °C, (c) 600 °C, (d) 800 °C and (e) 1000 °C. The asterisk (*) denotes the anatase Bragg peak positions, and the open circle (o) the rutile Bragg peak positions.

3. Results and discussion

3.1. Crystalline structure and transmittance

The GIXRD patterns of the synthesized TiO_2 films, heat treated at 400, 500, 600, 800 and 1000 °C, are illustrated in Fig. 1. It can be observed that the modified TiO_2 sample annealed at 400 °C is amorphous, whereas the annealing at 500 and 600 °C results in the development of anatase phase. With further increase of the annealing temperature to 800 °C, rutile phase is developed, with anatase remaining the dominant phase. According to the literature, the rutile phase appears at 700 °C [49] and it is almost completed at 800 °C. The measured 3% mass fraction of the rutile (Table 1) in the sample treated at 800 °C is considered low, as well as in the sample treated at 1000 °C where the rutile content is increased (by a factor of 7) but not completed. Brookite, which is the high temperature crystalline modification of TiO_2, was not found in the sample treated at 1000 °C. These results indicate that the modification with thiourea inhibits the anatase to rutile phase transformation of TiO_2.

The obtained average crystallite sizes (Table 1) reveal a small increase with temperature for anatase crystallites. The rutile crystallites appear at 800 °C with an important increase of their size at 1000 °C (58.4 nm), due to the phase transformation from anatase to rutile and the sintering phenomena which favour the growth of rutile.

The transmittance UV–vis spectra of the modified films are presented in Fig. 2. The spectra reveal that all the films absorb the electromagnetic radiation at wavelengths lower than 300 nm. The transmittance reaches approximately the value of 20% at a wavelength of 380 nm that corresponds to the band gap of TiO_2. A gradual increase in the transmittance is observed with increase of the wavelength and transmittance values of 60–70% are recorded for the wavelengths 600–900 nm. For the films heat treated at 500 and 600 °C, the transmittance values appear significantly reduced in comparison to those for the film treated at 400 °C. Further increase of the treatment temperature up to 1000 °C does not practically influence the transmittance of the films. In the films treated at 500 and 600 °C, the reduced transmittance can be attributed both to the diffuse light scattering in the films and the modification of TiO_2

Table 1
Phase and crystallite size of thiourea modified TiO_2 sol–gel thin films annealed at various temperatures.

Thermal treatment temperature [°C]	500	600	800		1000	
Phase Present	Anatase	Anatase	Anatase	Rutile	Anatase	Rutile
Average crystallite size [nm]	28.2	28.6	29.3	24.8	31.8	58.4
Phase content [%]	100	100	97.1	2.9	79.3	20.7

with thiourea. Finally, in the films prepared at higher temperatures, the diffuse scattering of the light becomes a major mechanism of the maintenance of the reduced transmittance values.

In addition, it is worth mentioning that interference fringes in 300–900 nm wavelength range, characteristic for thin films [50], were not observed.

3.2. Dark conductivity

As it is well known, the conductivity of TiO_2 is highly sensitive to the environment and can be affected by oxygen vacancies. These vacancies are intrinsic for any oxide material and act as electron donors, determining the TiO_2 n-type conductivity. In this section, the electrical conductivity in the dark of the thiourea modified TiO_2 sol–gel films, heat treated at various temperatures, is presented. The dark conductivity was measured both in air and a vacuum environment.

In order to determine the mechanism of electrical transport, detailed measurements of the dark conductivity (σ_d) as a function of the specimen's temperature in the range 300–410 K were performed, in vacuum (10^{-2} Pa) and in air. It is important to note that, because of the small thicknesses of the samples, the dark currents were smaller than the limit on measurements (<10^{-14} A).

In this respect, measurements were possible only in vacuum for the sample heat treated at 500 °C, and in both vacuum and air for the sample heat treated at 600 °C. The σ_d values in vacuum, at 330 K, are 4.3×10^{-8} and 6.99×10^{-9} Ω^{-1} m^{-1} for the samples thermally treated at 500 and 600 °C respectively, while the corresponding σ_d value in air for the sample thermally treated at 600 °C is 6.39×10^{-9} Ω^{-1} m^{-1} (Table 2). The difference in the σ_d values in vacuum (more than half an order of magnitude) for the treatment temperatures 500 and 600 °C can be assigned to thiourea modification that contributes to the increase of the electrical conductivity. Since the modification agents (N and S) escape gradually from the films with the increase of the treatment temperature [43,51], the additional donor states are significantly reduced causing a decrease in σ_d for the sample heat treated at 600 °C. For the heat treatment temperature of 600 °C, the σ_d value in air is slightly lower than that in vacuum, probably due to the competition between two mechanisms that act in air: (i) oxygen adsorption which causes the decrease of σ_d and (ii) water adsorption which increases it [52–54]. It is evident that the influence of oxygen adsorption prevails in this sample.

The activation energies E_a were calculated from the $\log \sigma_d$ versus 10^3/T Arrhenius plots obtained from the temperature dependent conductivity studies (Fig. 3). It was found that the activation is temperature dependent, indicating that band conduction is the main charge transport mechanism. The least squares fitting to the data in the high temperature regime gives the activation energies E_a (Table 2). It is well known that in anatase TiO_2, the free carriers arise from stoichiometric deviations, mainly due to oxygen vacancies located below the conduction band edge at 0.75–1.18 eV [55]. The decrease shown in the E_a value for the sample heat treated at 500 °C is attributed to the modification with thiourea, which causes the increase in electrical conductivity.

3.3. Photoconductivity

The study of the photoconductivity behavior is a useful tool for interpreting the competition among charges' photogeneration, recombination and trapping in semiconductors. In the present work, charge transport properties of thiourea modified TiO_2 thin sol–gel films have been studied, using transient photoconductivity measurements.

3.3.1. In vacuum

The transient photoconductivity σ_p of the thiourea modified TiO_2 nanocrystalline thin films in vacuum (10^{-2} Pa) is presented in Fig. 4. The σ_p values after 20 min of illumination are presented in Table 2. For the thermal treatment temperature of 400 °C [Fig. 4(a)], the rise is sharp, following an almost linear dependence, indicating that, during the illumination in vacuum, the recombination and thermal release rates follow the same change with time. It is worth mentioning that no evidence of saturation during the time of measurements is observed. The sample, at the end of the first

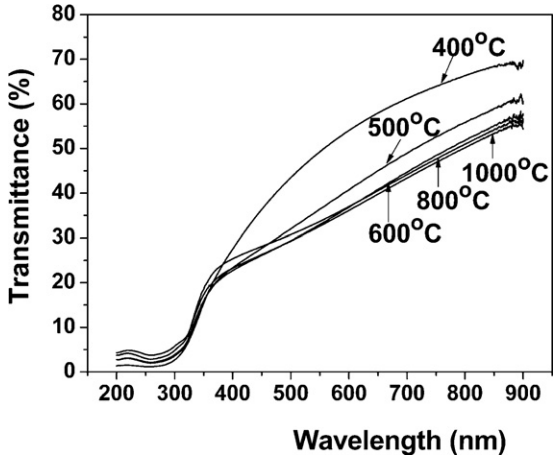

Fig. 2. UV–vis spectra of the thiourea modified TiO_2 films treated at various temperatures.

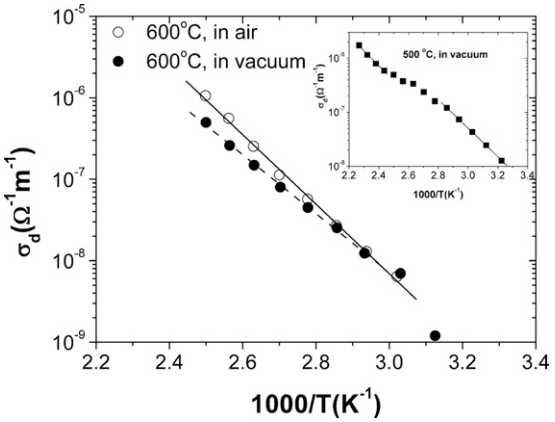

Fig. 3. Temperature dependence of the dark conductivity versus 10^3/T in vacuum and in air, plotted as $\log \sigma_d = f(10^3/T)$ for sample treated at 600 °C and the linear regression fits for the determination of the activation energies E_a. The temperature dependence of the dark conductivity in vacuum for sample treated at 500 °C is given as an inset of the figure.

Table 2
Electrical conductivity σ_d, activation energy E_a and photoconductivity σ_p of thiourea modified TiO_2 sol–gel thin films in vacuum and in air.

Thermal treatment temperature [°C]	400	500	600	800	1000
In vacuum, σ_d [Ω^{-1} m^{-1}]		4.3×10^{-8}	6.99×10^{-9}		
In air, σ_d [Ω^{-1} m^{-1}]			6.39×10^{-9}		
In vacuum, E_a [eV]		0.54	0.72		
In air, E_a [eV]			0.85		
In vacuum, σ_p [Ω^{-1} m^{-1}], after 20 min of illumination	5.35×10^{-6}	1.70	1.01×10^{-1}	1.75×10^{-6}	5.40×10^{-9}
In air, σ_p[Ω^{-1} m^{-1}], after 20 min of illumination	2.24×10^{-8}	2.5×10^{-3}	1.43×10^{-3}	9.73×10^{-7}	2.91×10^{-8}

illumination period, presents a low σ_p value, attributed to its amorphous structure. When the light is switched off, the decay is initially abrupt, suggesting that the recombination rate becomes important, but soon the increasing thermal release rate of the trapped electrons results in a lower decay rate. At the end of the second illumination period, σ_p reaches much higher values. This significant asymmetry between first and second rise originates from the fact that transient photoconductivity at the end of the first decay period has not taken its initial dark value yet [52,53].

The σ_p behavior for the sample heat treated at 500 °C is shown in Fig. 4(b). During the first and second rise it follows the usual sublinear trend [52]. After 20 min of illumination, σ_p reaches the high value of 1.70 Ω^{-1} m^{-1}, which is more than eight orders of magnitude higher than its σ_d value. The high values of σ_p suggest a high conduction band electron density which enhances the recombination rate. As a consequence, a decrease in the asymmetry between the first and second rise is observed, compared to the sample heat treated at 400 °C. When the light is switched off, a slow decay follows, due to the high thermal release rate from the traps.

The samples heat treated at 600, 800 and 1000 °C [Fig. 4(c)–(e)] show a significant decrease in their σ_p values with increase of the thermal treatment temperature. In comparison with the sample heat treated at 500 °C, a reduction of six and eight orders of magnitude is noticed for the heat treatment temperatures of 800 and 1000 °C respectively. As revealed by XRD analysis, the samples treated at 800 and 1000 °C exhibited a considerable increase in the grain size with a simultaneous rise in their rutile/anatase content. It has been reported that the recombination rate is enhanced when the grain size and the rutile/anatase ratio is increased [56,57]. The effect of an increased recombination rate at the first stages of illumination is obvious for the sample heat treated at 600 °C. In addition, a quasi saturation behavior is shown during the last stages of the illumination periods. As a consequence of the high recombination rate, lower values of σ_p during the second rise are obtained.

The decay for the samples heat treated at 600, 800 and 1000 °C occurs in a high rate, indicating that recombination is prevalent, and slows down only when the rate of the trapped electrons activated to the conduction band increases significantly.

3.3.2. In air

Fig. 5 illustrates the σ_p behavior at 300 K in air, of the thiourea modified samples heat treated at the five different temperatures, ranging from 400 to 1000 °C. The σ_p values in air after 20 min of illumination are presented in Table 2. As it can be observed, the σ_p values in air are several orders of magnitude lower than those in vacuum. The decrease is attributed to the shortening of the electron lifetime in air caused by the surface adsorbed oxygen gas molecules and the creation of a great number of electron scavengers O_2^- [58].

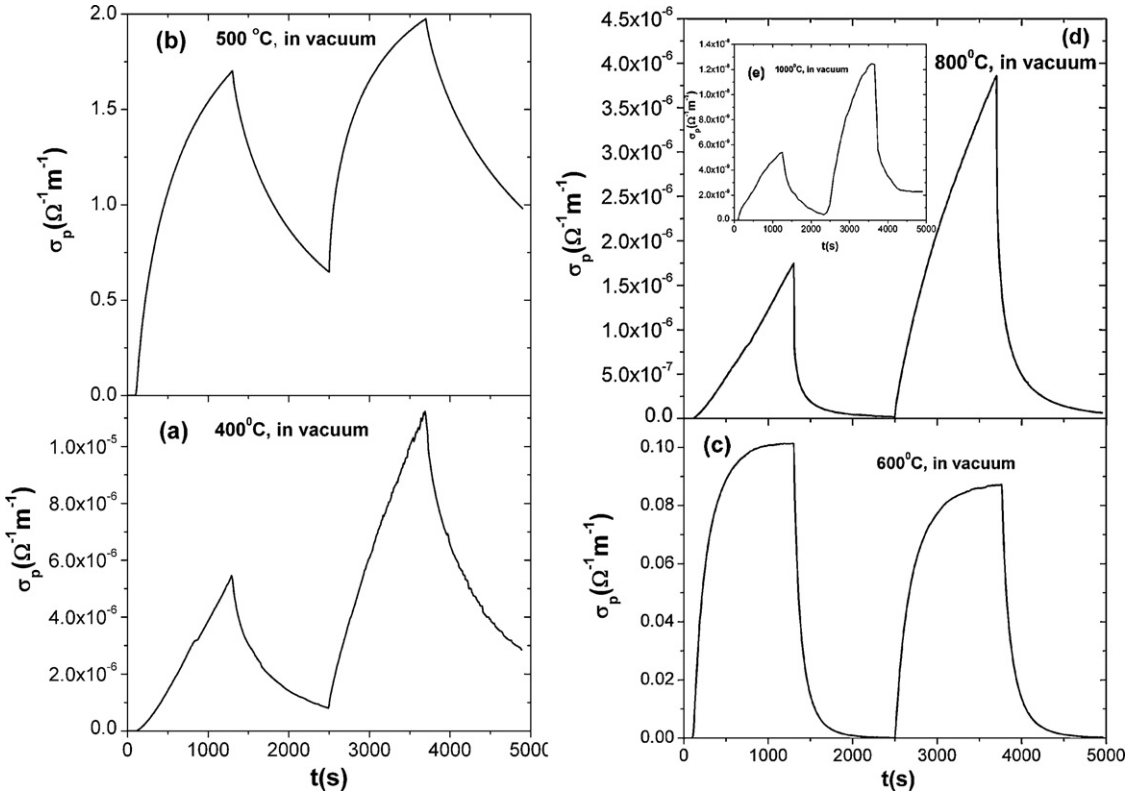

Fig. 4. The photoconductivity response at 300 K, in vacuum, under white light illumination of full intensity (F_o = 500 W/m^2) of the samples heat treated at: (a) 400 °C, (b) 500 °C, (c) 600 °C and (d) 800 °C. The photoconductivity response (e) of the sample heat treated at 1000 °C is given as an inset of (d).

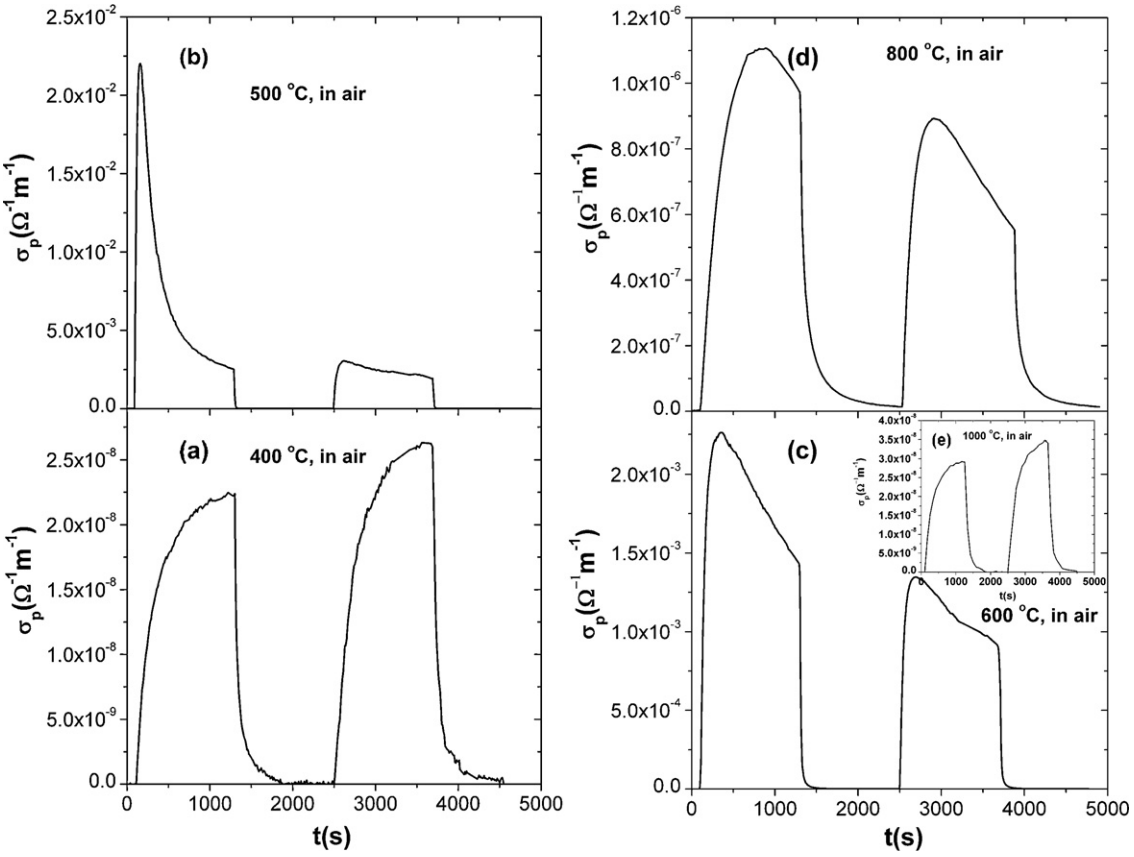

Fig. 5. The photoconductivity response at 300 K, in air, under white light illumination of full intensity (F_o = 500 W/m^2) of the samples heat treated at: (a) 400 °C, (b) 500 °C, (c) 600 °C and (d) 800 °C. The photoconductivity response (e) of the sample heat treated at 1000 °C is given as an inset of (c).

For the thermal treatment temperature of 400 °C [Fig. 5(a)], the rise during the first illumination period follows the usual sublinear trend. The σ_p value, after 20 min of illumination is more than three orders of magnitude lower than the corresponding value in vacuum. The σ_p falls off rapidly when the light is turned off, suggesting the domination of recombination in air, and the decay slows down only when the thermal release rate becomes important.

In the case of 500 °C [Fig. 5(b)], the σ_p versus time plot is quite different. The recombination rate dominates from the early stages of illumination, while σ_p rises quickly to a maximum value and then decreases rapidly. An increase of five orders of magnitude in σ_p compared with the case of the heat treatment temperature of 400 °C is shown, which is attributed to the amorphous structure of the modified TiO_2 films at 400 °C. The high recombination rate becomes determinant during the second illumination period, not permitting photoconductivity to reach high values.

The σ_p behavior of the samples heat treated at 600 °C, 800 °C and 1000 °C is shown in Fig. 5(c)–(e), respectively. A further significant drop in σ_p values occurs due to the additional recombination centers created with the increase of crystallite size and rutile content [59].

Photoconductivity of the thiourea modified samples at the end of the first illumination period as a function of the thermal treatment temperature is shown in Fig. 6. The values are obtained at 300 K, both in vacuum and in air.

The sample treated at 400 °C is characterized by low σ_p values, attributed to the amorphous structure of the film. For thermal treatment temperatures higher than 500 °C an effective decrease of σ_p results. It seems that the heat treatment temperature of 500 °C is the optimum choice for achieving high σ_p values in thiourea modified films.

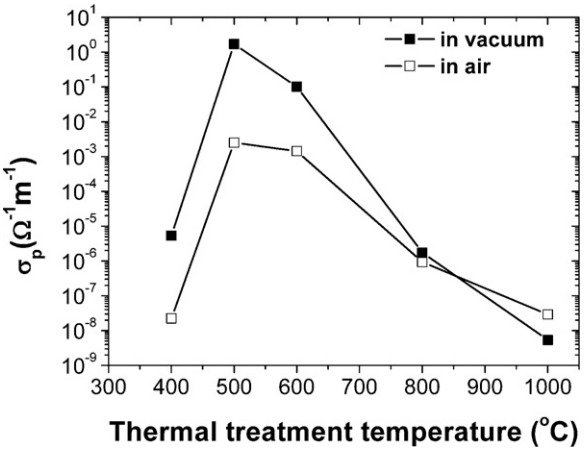

Fig. 6. The photoconductivity at the end of the first illumination period, at 300 K, versus the different temperatures of thermal treatment, in vacuum and in air.

4. Conclusions

The effect of thermal treatment temperature on the microstructure, UV–vis transmittance, electrical conductivity and transient photoconductivity of thiourea modified nanocrystalline sol–gel TiO_2 films was investigated. In addition, the influence of the environment on conductivity and photoconductivity was studied.

The films exhibited amorphous, anatase and mixed anatase/rutile structure, depending on the heat treatment temperature. The presence of thiourea inhibited the anatase to

rutile phase transformation of TiO_2. The reduced transmittance of the TiO_2 films was attributed to both the thiourea modification and the light scattering in the films.

Furthermore, the heat treatment at 500 °C results in lower thermal activation energy E_a due to the new states above the valence band of TiO_2 introduced through the thiourea addition. In air, the photoconductivity is reduced three orders of magnitude more than that in vacuum, because of the adsorbed oxygen. The transient photoconductivity behavior of the samples in air suggests the prevalent role of the recombination rate. The decrease of σ_p values by several orders of magnitude when the treatment temperature is increased is ascribed to the considerable increase in the crystallite sizes and the simultaneous rise in the rutile/anatase ratio. To summarize, the heat treatment at 500 °C yields the optimum results for the achievement of high photoconductivity in thiourea modified films.

Acknowledgement

The authors would like to thank Dr Nikos Spiliopoulos for the evaporation of the electrodes on the samples.

References

[1] U. Diebold, Appl. Phys. A 76 (2002) 1.
[2] A.J. Frank, N. Kopidakis, J. van de Lagemat, Coord. Chem. Rev. 248 (2004) 1165.
[3] L.R. Sheppard, T. Bak, J. Nowotny, M.K. Nowotny, Int. J. Hydrogen Energy 32 (14) (2007) 2660.
[4] N. Yamada, T. Hitosugi, N.L.H. Hoang, Y. Funabayashi, Y. Hirose, S. Konuma, T. Shimada, T. Hasegawa, Thin Solid Films 516 (2008) 5754.
[5] D. Joskowska, K. Pomoni, A. Vomvas, B. Kościelska, D.L. Anastassopoulos, J. Non-Cryst. Solids 356 (37–40) (2010) 2042.
[6] K. Tonooka, N. Te-Wei Chiu, Kikuchi, Appl. Surf. Sci. 255 (2009) 9695.
[7] A.R. Bally, E.N. Korobeinikova, P.E. Schmid, F. Lévy, F. Bussy, J. Phys. D 31 (1998) 1149.
[8] A. Yildiz, F. Iacomi, D. Mardare, J. Appl. Phys. 108 (2010) 083701.
[9] F. Yakuphanoglu, M. Okutan, K. Korkmaz, J. Alloys Compd. 450 (2008) 39.
[10] D. Mardare, G.I. Rusu, F. Iacomi, M. Girtan, I.V. Simiti, Mater. Sci. Eng. B 118 (2005) 187.
[11] K. Pomoni, A. Vomvas, Chr. Trapalis, J. Non-Cryst. Solids 354 (35–39) (2008) 4448.
[12] H. Kitagawa, T. Kunisada, Y. Yamada, S. Kubo, J. Alloys Compd. 508 (2) (2010) 582.
[13] Y. Su, S. Han, X. Zhang, X. Chen, L. Lei, Mater. Chem. Phys. 110 (2008) 239.
[14] B. Tian, C. Li, F. Gu, H. Jiang, Y. Hu, J. Jhang, Chem. Eng. J. 151 (2009) 220.
[15] M. Asiltürk, F. Saylikan, E. Arpa, J. Photochem. Photobiol. A 203 (2009) 64.
[16] B. Gao, T.M. Lim, D.P. Subagio, T.T. Lim, Appl. Catal. A: Gen. 375 (2010) 107.
[17] R. Sasikala, A.R. Shirole, V. Sudarsan, V. Jagannath, C. Sudakar, R. Naic, R. Rao, S.R. Bharadwaj, Appl. Catal. A: Gen. 377 (2010) 47.
[18] G.Q. Wang, W. Lan, G.J. Han, Y. Wang, Q. Su, X.Q. Liu, J. Alloys Compd. 509 (10) (2011) 4150.
[19] W. Choi, A. Termin, M.R. Hoffman, J. Phys. Chem. 98 (1994) 13669.
[20] F.B. Li, X.Z. Li, M.F. Hou, Appl. Catal. B: Environ. 48 (2004) 185.
[21] B. Naik, K.M. Parida, C.S. Gopinath, J. Phys. Chem. 114 (2010) 19473.
[22] R. Asahi, T. Morikawa, T. Ohwaki, K. Aoki, Y. Taga, Science 293 (2001) 269.
[23] J.C. Yu, J.G. Yu, W.K. Ho, Z.T. Jiang, L.Z. Jiang, Chem. Mater. 14 (2002) 3808.
[24] T. Umebayashi, T. Yamaki, H. Itoh, K. Asai, Appl. Phys. Lett. 81 (2002) 454.
[25] T. Ohno, M. Akiyoshi, T. Umebayashi, K. Asai, T. Mitsui, M. Matsumura, Appl. Catal. A: Gen. 265 (2004) 115.
[26] M. Shen, Z. Wu, H. Huang, Y. Du, Z. Zou, P. Yang, Mater. Lett. 60 (2006) 693.
[27] S. In, A. Orlov, R. Berg, F. Garcia, S. Pedrosa-Jimenez, M.S. Tikhov, D.S. Wright, R.M. Lambert, J. Am. Chem. Soc. 129 (2007) 13790.
[28] A. Zaleska, J.W. Sobczak, E. Grabowska, J. Hupka, Appl. Catal. B- Environ. 78 (2008) 92.
[29] J. Yu, S. Lin, Z. Xiu, W. Yu, G. Feng, J. Alloys Compd. 471 (2009) L23.
[30] Y. Lv, L. Yu, H. Huang, H. Liu, Y. Feng, J. Alloys Compd. 488 (2009) 314.
[31] Z. Liu, Y. Wang, W. Chu, Z. Li, C. Ge, J. Alloys Compd. 501 (2010) 54.
[32] D. Wu, M. Long, W. Cai, C. Chen, Y. Wu, J. Alloys Compd. 502 (2010) 289.
[33] J. Wang, Z. Wang, H. Li, Y. Gui, Y. Du, J. Alloys Compd. 494 (2010) 372.
[34] M.R. Bayati, A.Z. Moshfegh, F. Golestani-Fard, Appl. Catal. A: Gen. 389 (2010) 60.
[35] S. Bangkedphol, H.E. Keenan, C.M. Davidson, A. Sakultantimetha, W. Sirisaksoontorn, A. Songsasen, J. Hazard. Mater. 184 (1–3) (2010) 533.
[36] C.M. Teh, A.R. Mohamed, J. Alloys Compd. 509 (2011) 1648.
[37] L. Szatmáry, S. Bakardjieva, J. Šubrt, P. Bezdička, J. Jirkovský, Z. Bastl, V. Brezová, M. Korenko, Catal. Today 161 (2011) 23.
[38] T. Lindgren, J.M. Mwabora, E. Avendaño, J. Jonsson, A. Hoel, C. Granqvist, S. Lindquist, J. Phys. Chem. B 107 (24) (2003) 5709.
[39] J. Lee, J. Park, J. Cho, Appl. Phys. Lett. 87 (1) (2005) (1–1).
[40] Q.L. Chen, G. Zheng, H.H. He, B. Li, Mod. Phys. Lett. B 25 (2011) 119.
[41] V.N. Kuznetsov, N. Serpone, J. Phys. Chem. B 110 (2006) 25203.
[42] Y. Yalcin, N. Kilic, Z. Cinar, J. Adv. Oxid. Technol. 13 (2010) 281.
[43] X. Li, R. Xiong, G. Wei, Catal. Lett. 125 (2008) 104.
[44] H. Li, J. Wang, H. Li, S. Yin, T. Sato, Res. Chem. Intermed. 36 (2010) 27.
[45] O. Carp, C.L. Huisman, A. Reller, Prog. Solid State Chem. 32 (2004) 33.
[46] N. Todorova, T. Giannakopoulou, G. Romanos, T. Vaimakis, J.G. Yu, C. Trapalis, Int. J. Photoenergy 2008 (2008) ID 534038.
[47] T. Giannakopoulou, N. Todorova, P. Osiceanu, A. Lagoyannis, T. Vaimakis, C. Trapalis, Thin Solid Films 517 (24) (2009) 6694.
[48] R.A. Spurr, H. Myers, Anal. Chem. 29 (1957) 760.
[49] J.G. Yu, H.G. Yu, B. Cheng, X.J. Zhao, J.C. Yu, W.K. Ho, J. Phys. Chem. B 107 (2003) 13871.
[50] T. Giannakopoulou, N. Todorova, T. Vaimakis, S. Ladas, C. Trapalis, J. Sol. Energy Eng. 130 (2008) 041007.
[51] P. Periyat, D.E. McCormack, S.J. Hinder, S.C. Pillai, J. Phys. Chem. C 113 (2009) 3246.
[52] K. Pomoni, A. Vomvas, Chr. Trapalis, Thin Solid Films 516 (2008) 1271.
[53] A.M. Eppler, I.M. Ballard, J. Nelson, Physica E 14 (2002) 197.
[54] A. Tilocca, A. Selloni, J. Phys. Chem. B 108 (15) (2004) 4743.
[55] D.C. Cronemeyer, Phys. Rev. 113 (1959) 1222.
[56] M. Hamadanian, A. Reisi-Vanani, A. Majedi, Appl. Surf. Sci. 256 (2010) 1837.
[57] C. Colbeau-Justin, M. Kunst, D. Huguenin, J. Mater. Sci. 38 (2003) 2429.
[58] N. Golego, S.A. Studenikin, M. Cocivera, Phys. Rev. B 61 (2000) 8262.
[59] P. Górska, A. Zaleska, E. Kowalska, T. Klimczuk, J.W. Sobczak, E. Skwarek, W. Janusz, J. Hupka, Appl. Catal. B: Environ. 84 (2008) 440.